ADVANCED FUNCTIONAL MATERIALS

www.afm-journal.de

# Scaling Effects on the Electrochemical Performance of poly(3,4-ethylenedioxythiophene (PEDOT), Au, and Pt for Electrocorticography Recording

*Mehran Ganji, Ahmed T. Elthakeb, Atsunori Tanaka, Vikash Gilja, Eric Halgren, and Shadi A. Dayeh**

**Reduced contact size would permit higher resolution cortical recordings, but the effects of diameter on crucial recording and stimulation properties are poorly understood. Here, the first systematic study of scaling effects on the electrochemical properties of metallic Pt and Au and organic poly(3,4-ethylenedioxythiophene):polystyrene sulfonate (PEDOT:PSS) electrodes is presented. PEDOT:PSS exhibits better faradaic charge transfer and capacitive charge coupling than metal electrodes, and these characteristics lead to improved electrochemical performance and reduced noise at smaller electrode diameters. PEDOT:PSS coating reduces the impedances of metallic electrodes by up to 18x for diameters <200 µm, but has no effect for millimeter scale contacts due to the dominance of series resistances. Therefore, the performance gains are especially significant at smaller diameters and lower frequencies essential for recording cognitive and pathological activities. Additionally, the overall reduced noise of the PEDOT:PSS electrodes enables a lower noise floor for recording action potentials. These results permit quantitative optimization of contact material and diameter for different electrocorticography applications.**

## 1. Introduction

The high selectivity, sensitivity and longevity of neuronal interface devices are dependent upon design considerations such as size, shape, and morphology of the applied materials.[1] The specific electrochemical, physical (mechanical), and biological characteristics of electrophysiology devices play a direct role in achieving advanced neuronal interface standards. In particular, for neuronal probes in the form of microelectrode arrays and neuroprosthetic devices, recording quality is inversely proportional to electrode impedance at the tissue interface.[2] For large scale recording of neuronal and field activities, sampling at a high spatiotemporal resolution[1b,3] calls for smaller microelectrode sites in order to support higher channel count while increasing spatial specificity and in maintaining the electrode/electrolyte interface at low impedance. However, decreasing electrode dimensions reduces the device's electrochemically active area and increases the electrochemical impedance, which in turn can compromise the recording quality. This compromise is mostly attributed to the rise of noise voltage at the electrode/electrolyte interface that is directly proportional to the electrode impedance.[4] Given the low magnitude of neuronal potentials, their content can be screened by a high noise floor due to the random ion fluctuations in an electrophysiological medium.[2b] The mixed electronic/ionic conductivity of conducting polymers, particularly of poly(3,4-ethylenedioxythiophene):polystyrene sulfonate (PEDOT:PSS),[5] readily reduces the electrochemical impedance enabling smaller geometrical design with possibly uncompromised signal quality.[6]

Despite several decades of research in neuronal interface technologies, the scaling laws of the electrochemical characteristics of neuronal probes (i.e., their functional dependencies on size) have not been systematically determined. Here, we conducted a parametric study to evaluate scaling effects on the electrochemical performance of PEDOT:PSS on Au, PEDOT:PSS on Pt, pure Au and pure Pt electrodes with diameters ranging from 20 to

M. Ganji, A. T. Elthakeb, Prof. V. Gilja, Prof. S. A. Dayeh
Department of Electrical and Computer Engineering
University of California San Diego
La Jolla, CA 92093, USA
E-mail: sdayeh@eng.ucsd.edu

A. Tanaka, Prof. S. A. Dayeh
Materials Science and Engineering Program
University of California San Diego
La Jolla, CA 92093, USA

Prof. V. Gilja
Neurosciences Program
University of California San Diego
La Jolla, CA 92096, USA

Prof. E. Halgren
Departments of Radiology and Neuroscience
University of California San Diego
La Jolla, CA 92103, USA

Prof. S. A. Dayeh
Department of NanoEngineering
University of California San Diego
La Jolla, CA 92093, USA

The ORCID identification number(s) for the author(s) of this article can be found under https://doi.org/10.1002/adfm.201703018.

**DOI: 10.1002/adfm.201703018**

 

2000 µm. We quantify series resistance in its electrochemical and electrode lead components, as well as the capacitive and faradaic components of the overall electrode impedance. Equations are derived to predict these values as a function of diameter for each electrode material, thus permitting calculation of how their performance scales at smaller diameters. We also show that the electrochemical component that dominates electrode impedance varies across the frequency bands commonly sampled in clinical and functional studies. We then benchmark the impedances as a function of diameter in the different brain-wave frequency bands and illustrate performance gains for PEDOT:PSS coated electrodes in these different frequency regimes. Finally, we characterize the three-terminal noise performance and depict their diameter and frequency dependencies for all electrode materials. These results provide new insight into electrochemical coupling with these different electrode materials.

## 2. Result and Discussion

Microelectrodes with different interface materials including Au, PEDOT:PSS/Au, Pt, and PEDOT:PSS/Pt were fabricated on ultrathin (3.8 µm) flexible parylene C substrates as shown in **Figure 1**a. The details of the fabrication are described in the Experimental Section following previously published procedures.[5a] The thin parylene C layers were used as a substrate-carrier and passivation layers, each is 1.9 µm thick, to enable a microelectrode array that conforms to the cortical surface when used in vivo—for better coupling of brain activity and higher signal to noise ratio (SNR) recordings.[7] Electrode contacts were connected to the external characterization circuitry via 20 µm wide and 10/100 nm thick Ti/Au wire leads, with Au being on top of Ti, and an ACF/ribbon cable (Figure 1a). To assess the scaling of the microelectrodes' electrochemical properties, 16 different electrode diameters ranging from 2000 (macrodot) down to 20 µm (microdot) were studied. The cross-sectional scanning electron microscope (SEM) image in Figure 1b where the electrode edge was sliced by focused ion beam (FIB) shows full encapsulation of the metal leads with parylene C and exposure of the evaporated surface in the microdot electrode contact. This contact has a surface roughness of ≈12 nm measured by atomic force microscopy (AFM) as shown in Figure S1 (Supporting Information). The Au surface is ≈1.9 µm below the parylene C surface. This also applies

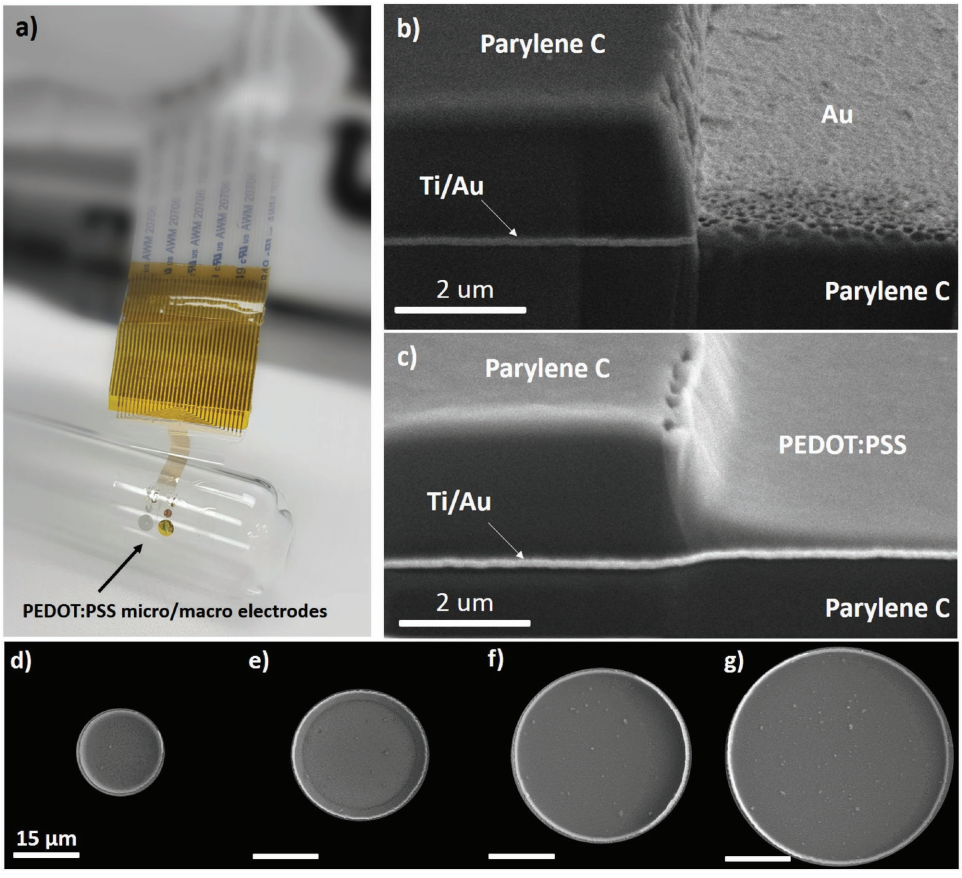


**Figure 1.** Structure and morphology of studied ECoG devices. a) A picture of the fabricated PEDOT:PSS/Au ECoG electrodes on 3.8 µm thick parylene C substrate that were bonded using anisotropic conductive filament (ACF) to ribbon cables for characterization. 16 different diameters ranging from 2000 to 20 µm were included in each device. b) 45° angle view of a cross-sectional SEM image after FIB slicing of an Au microelectrode edge and showing parylene C encapsulating the metal leads, and an exposed Au interface layer that is ≈1.9 µm below the parylene C external surface. c) 45° angle view of a cross-sectional SEM image after FIB slicing of a PEDOT:PSS/Au microelectrode displaying a uniform coating of the PEDOT:PSS layer on top of the underlying exposed Au contact. Top view SEM images of d) the 20 µm, e) 30 µm, f) 40 µm, and g) 50 µm PEDOT:PSS/Au electrodes.

for the PEDOT:PSS devices except that the microdot areas displayed negligible surface roughness of ≈5 nm, measured also by AFM. Also, PEDOT:PSS coated the edge of the parylene C sidewalls as shown in Figure 1c. Figure 1d–g show top view SEMs of different PEDOT:PSS/Au electrodes with 20, 30, 40, and 50 µm diameters. In general, we observed no significant morphological differences for dots with different diameters. As can be observed in Figure 1c, there is a larger thickness of the PEDOT:PSS at the edge of the parylene C than at the surface of the Au layer. Using a surface profilometer (Figure S2a, Supporting Information), we observed that the thickness of the PEDOT:PSS does not change with diameter and that the edge thickness remains invariant for all studied diameters (Figure S2b, Supporting Information).

The analysis performed in this work is centered around the electrochemical impedance spectroscopy (EIS) that was performed in a three-electrode configuration in the frequency range of 1–$10^4$ Hz (see the Experimental Section). **Figure 2**a,b show the impedance magnitude and phase spectra of Au electrodes. As expected, by decreasing the electrode diameter and therefore decreasing the effective surface area, the electrochemical impedance values are increased. The impedance values at 1 kHz (commonly used to infer impedances at the frequency of an action potential [8]) varied from sub 1 kΩ to above 1 MΩ for diameters of 2000–20 µm, respectively. For diameters smaller than 100 µm, the Au electrodes showed capacitive-like behavior with phase spectra close to 90° across the whole frequency range. For diameters larger than 100 µm, a transition to ohmic-like characteristic is observed at higher frequencies where the overall impedance is dominated by series resistances. Figure 2c,d show the impedance magnitude and phase spectra of PEDOT:PSS/Au electrodes. It is evident that with using the organic PEDOT:PSS coating, the magnitude spectra are lower than those of the Au electrodes for the overall frequency range. For all studied diameters (down to 20 µm), the impedance values at 1 kHz were lower than 100 kΩ. Due to the overall lower impedance of PEDOT:PSS with respect to that of Au, the transition from the capacitive regime to the series-resistance dominant regime occurs at lower frequencies for PEDOT:PSS. Pt exhibited a similar impedance trend (Figure 2e) but slightly lower impedances than that of Au and the phase spectra showed a mixed capacitive-ohmic-like characteristics (Figure 2f) as discussed below. When PEDOT:PSS was coated on Pt, similar impedance spectra (Figure 2g) and phase (Figure 2h) were obtained to that of PEDOT:PSS on Au with a series resistance saturation floor that is higher than that on Au.

These data were used to model the electrochemical characteristics of the studied materials using the circuits shown in **Figure 3**a for Au and PEDOT:PSS and in Figure 3b for Pt, by simultaneously fitting the impedance spectra and Nyquist plots. The models comprise a constant phase element (CPE) that accounts for the double-layer capacitance, which is a nonideal capacitor with reactance $|X|_{\mathrm{CPE}} = \frac{1}{(2\pi f)^n C}$. The nonideal frequency dependence (i.e., $n < 1$) as opposed to that of ideal capacitors ($n = 1$) is often associated with inhomogeneities in the electrode surface roughness.[2b,9] The redox reaction resistance, $R_{\mathrm{ct}}$, accounts for the resistance to the direct charge transfer from solution to the electrode material through redox reactions, also commonly known as faradaic reactions. $C_{\mathrm{ad}}$ represents the adsorption capacitance, which accounts for the adsorption of the transferred species through the double layer on the electrode surface, which then participates in a redox reaction. $R_{\mathrm{s}}$ represents the series resistance that is composed of a solution resistance between the electrode surface and the counter electrode, the current crowding resistance near the electrode, usually at its edges,[2b] and the metal lead series resistances. Consistent with previous studies,[2b] we did not use an adsorption capacitance for Pt because the faradaic impedance, $Z_{\mathrm{f}}$, is usually much higher than the reactance of the capacitive branch, $|X|_{\mathrm{CPE}}$, as discussed below. This high impedance suggests that weak redox reactions and negligible adsorption of ion species occur at the surface of Pt electrodes. Indeed, the variability observed in the impedances of 50 µm diameter Pt microelectrodes[10] supports the weak and variable adsorption of ion species to the Pt surface. These models fit the impedance spectra and the Nyquist plots for all diameters within an average error of ±3% for Au, ±5.2% for PEDOT:PSS/Au, ±6.9% for Pt, and ±9.2% for PEDOT:PSS/Pt. The accuracy of the models in capturing the electrochemical characteristic of devices with different diameters is reflected in the good fits shown for three different diameters (60, 300, and 1000 µm) in Figure 3c–p for all studied materials.

With these EIS spectra and the model, we can now study the influence of scaling on each component of the electrochemical interface. The extracted values for material-specific series resistance ($R_{\mathrm{s}}$) are plotted versus diameter in semilog (**Figure 4**a) and log scales (Figure 4b), together with the best fit for their diameter dependence. The same data are plotted as a function of geometrical surface area (GSA) in Figure S3 (Supporting Information). The PEDOT:PSS coating did not influence $R_{\mathrm{s}}$. The functional dependence and the lowest $R_{\mathrm{s}}$ value at larger diameters were merely determined by the underlying metal electrode. This is not surprising as the ion permeability of PEDOT facilitates the interaction with underlying metal lead when other processes (capacitive and faradaic) are not limiting particularly at larger diameters. The $R_{\mathrm{s}}$ exhibited a $1/D$ dependence for Au and PEDOT:PSS/Au microelectrodes originating from current crowding at the edges of the dots with increased diameter, i.e., the electrochemical current transport occurs at the edge of the dots. Similarly, $R_{\mathrm{s}}$ for PEDOT:PSS/Pt and Pt exhibited a $1/D$ dependence for $D < 300$ µm above which $R_{\mathrm{s}}$ nearly saturates at ≈2 kΩ, the metal lead series resistance. Indeed, on a different set of samples that were fabricated at the same time, we observed that the two-point probe electrical series resistance of the metal leads is larger for Pt than that of Au (Figure S4, Supporting Information). Therefore, the overall diameter dependence for $R_{\mathrm{s}}$ of Pt and PEDOT:PSS/Pt can be fitted with $1/D^{1.75}$ masked by a diameter-independent series resistance. Since the larger contacts were more distant than the smaller contacts (Figure S4c, Supporting Information), the metal lead resistance is larger than those of larger contacts as shown in Figure S4a,b (Supporting Information). Therefore, we conclude that the electrochemical component of the series resistance scales as a function of $1/D$. As the diameter-independent series resistance of the metal leads becomes larger than this electrochemical series resistance, the functional dependence deviates to larger power exponent for $D$ as we observed for the case of PEDOT:PSS/Pt and Pt.

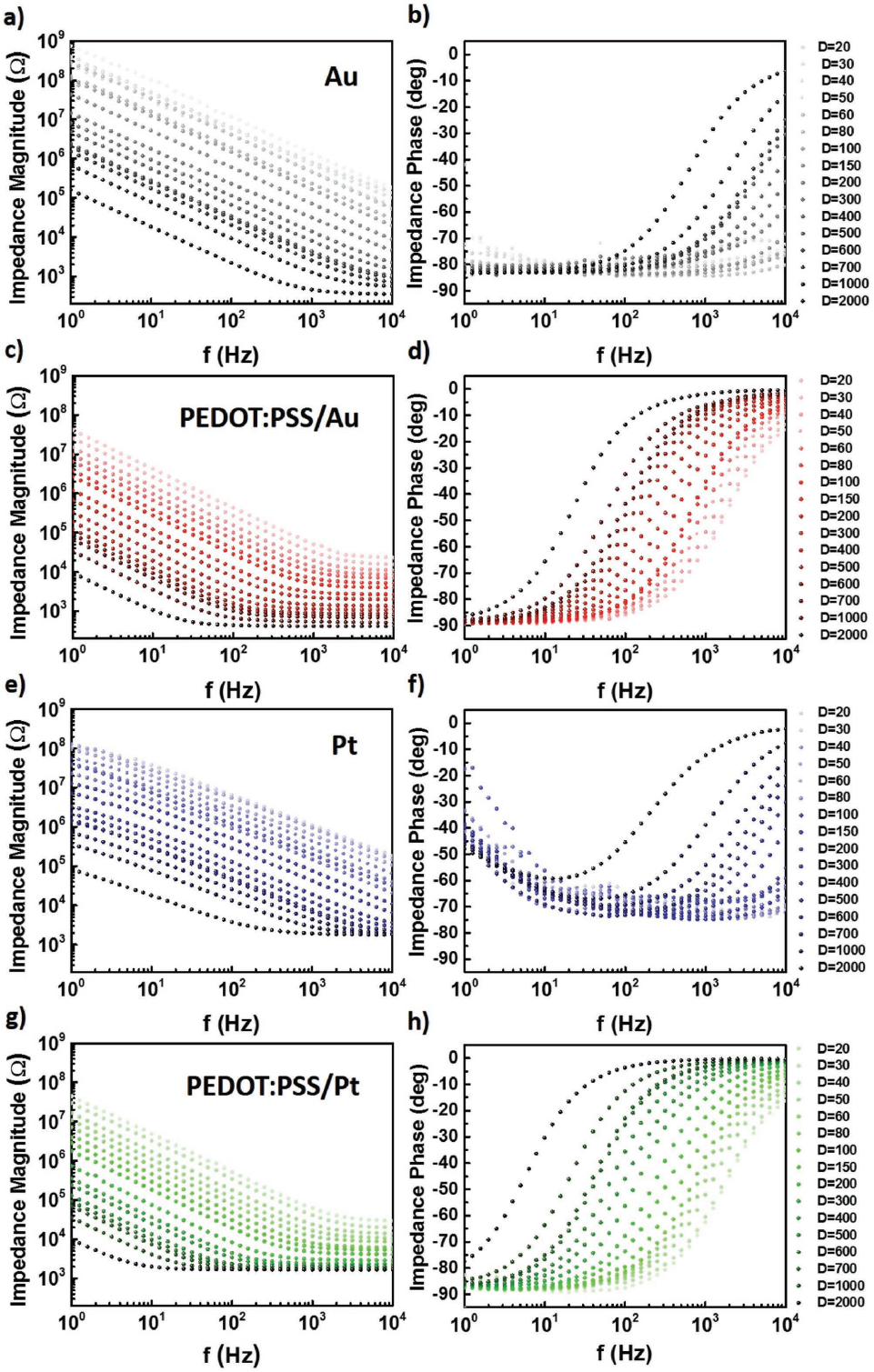


**Figure 2.** Electrochemical impedance spectra (EIS) of Au, PEDOT:PSS/Au, Pt, and PEDOT:PSS/Pt, with diameters ranging from 20 to 2000 µm. Magnitude and phase spectra of a,b) Au, c,d) PEDOT:PSS/Au, e,f) Pt, and g,h) PEDOT:PSS/Pt electrodes. The graded light to dark colors denote spectra at increasing diameters.

The scaling of the capacitive coupling embodied in CPE is shown in Figure 4c (semilog) and Figure 4d (log scale). Here, the reactance, $|X|_{\mathrm{CPE}} = \frac{1}{(2\pi f)^n C}$, was calculated at 1 kHz exhibiting an areal dependence of $1/D^2$ for Au and PEDOT:PSS/Au and slightly weaker/inhomogeneous areal dependence for Pt and PEDOT:PSS/Pt that exhibited $1/D^{1.75}$ and $1/D^{1.5}$, respectively.

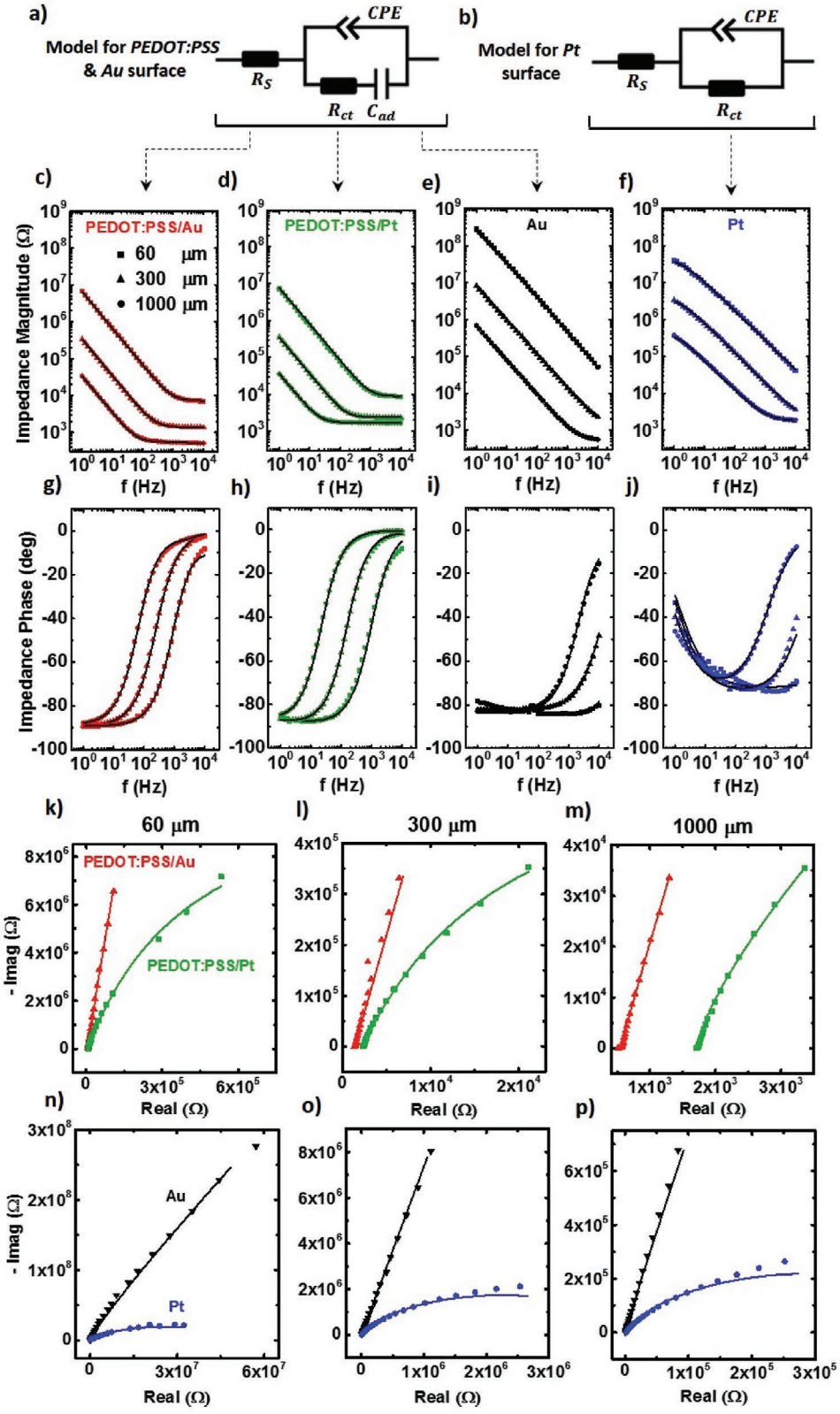


**Figure 3.** Fitting EIS and Nyquist plots of different scaled electrode materials using equivalent electrochemical circuit models. a) Equivalent circuit model for scaled PEDOT:PSS/Au, PEDOT:PSS/Pt, and Au electrodes. b) Equivalent circuit model for scaled Pt electrodes. c–f) Measured and fitted impedance magnitude spectra of 60, 300, and 1000 µm PEDOT:PSS/Au (red), PEDOT:PSS/Pt (green), Au (black), and Pt (blue) electrodes . g–j) Measured and fitted impedance phase spectra of 60, 300, and 1000 µm PEDOT:PSS/Au (red), PEDOT:PSS/Pt (green), Au (black), and Pt (blue) electrodes. Measured and fitted Nyquist plots of k–m) 60, 300, and 1000 µm PEDOT:PSS/Au (red) and PEDOT:PSS/Pt (blue), and n–p) Au (black) and Pt (blue) electrodes.

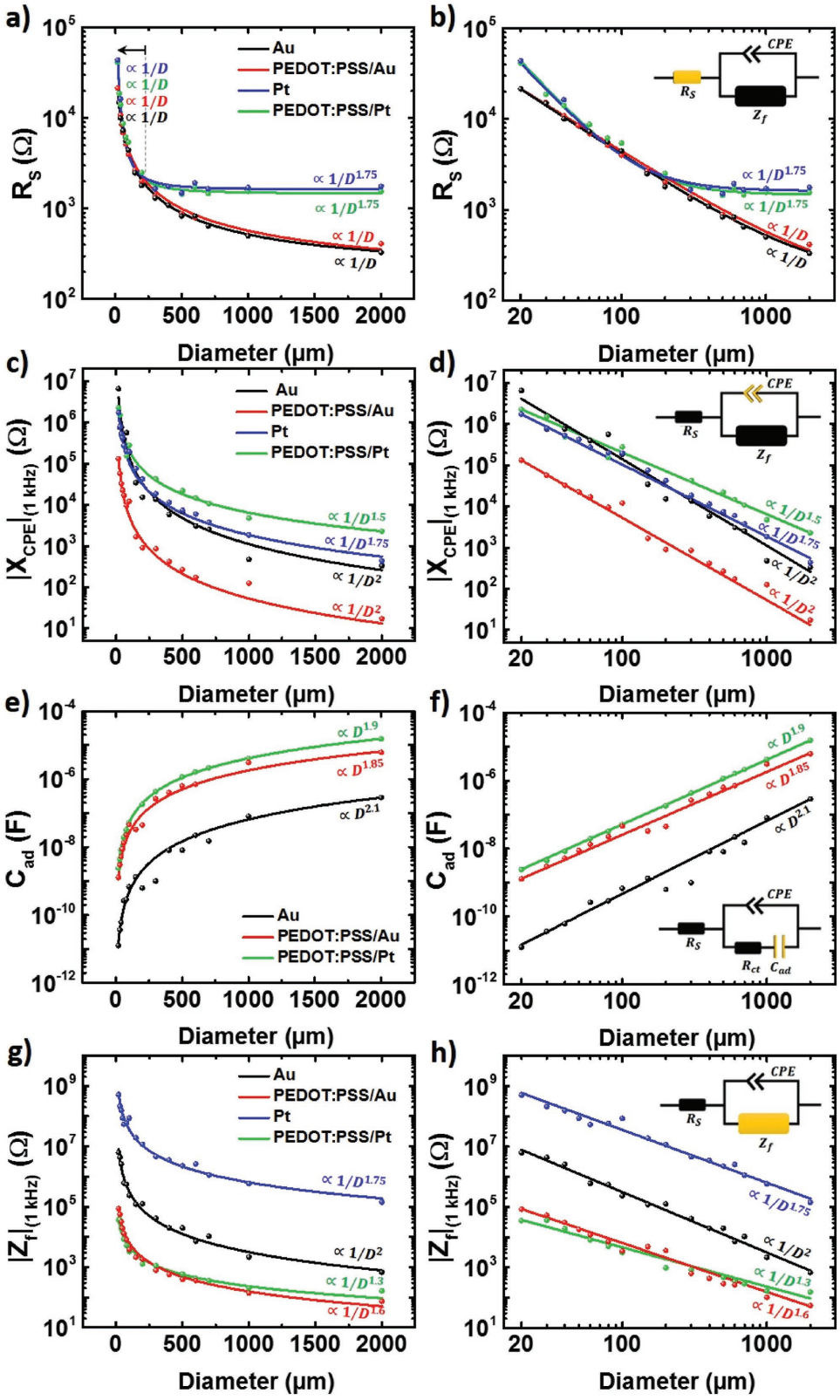


**Figure 4.** Effects of electrode diameter on specific electrochemical components of the electrode interface. a,b) Series resistance is greater for large diameter Pt electrodes (blue and green lines compared to red and black), independent of PEDOT:PSS coating (red vs black and green vs blue lines). c,d) CPE reactance at 1 kHz is least for PEDOT:PSS/Au electrodes at all diameters. e,f) Adsorption capacitance is increased in PEDOT:PSS coated contacts. g,h) Faradaic branch impedance (at 1 kHz) capacitance is decreased in PEDOT:PSS coated contacts. Extracted and fitted values are shown in semilog (a, c, e, g) and log (b, d, f, h) scales.

From the fits in Figure 3, $n$ was found to range from 0.73-0.91 for Au, 0.76-0.85 for Pt, 0.96-1 for PEDOT:PSS/Au, and 0.6-0.8 for PEDOT:PSS/Pt. PEDOT:PSS/Au exhibited the largest capacitive coupling characteristics (smallest $|X|_{CPE}$), whereas PEDOT:PSS/Pt exhibited the smallest capacitive coupling characteristics (largest $|X|_{CPE}$) at 1 kHz. The adsorption capacitance, $C_{ad}$, exhibited nearly two orders of magnitude larger value for PEDOT:PSS on both Au and Pt compared to that of Au across all diameters as shown in Figure 4e, where a nearly area-dependent scaling of $1/D^2$ was observed. To assess the impedance of the whole Faradaic branch (the serial combination of $R_{ct}$ and $|X|_{Cad}$ except for Pt), we calculated and plotted $Z_f$ at 1 kHz in Figure 4g,h. $Z_f$ is the largest for Pt, and is reduced by ≈1000× with PEDOT:PSS coating for all diameters. The Faradaic impedance of PEDOT:PSS is lowest on Au and Pt, highlighting the facilitation of the redox reaction by PEDOT:PSS coating. For a given electrode diameter, Au exhibited ≈100× higher $Z_f$ than Pt and ≈10 000× larger than that of PEDOT:PSS on either Au or Pt.

To highlight the differences in the net electrochemical impedance, we plotted in **Figure 5**a,b the 1 kHz magnitude of the impedance as a function of electrode diameter for all studied materials. The same plots are exhibited as a function of GSA in Figure S5 (Supporting Information). For smaller diameters, the PEDOT:PSS coating reduces the impedance by over ten times and the impedance for the larger diameter

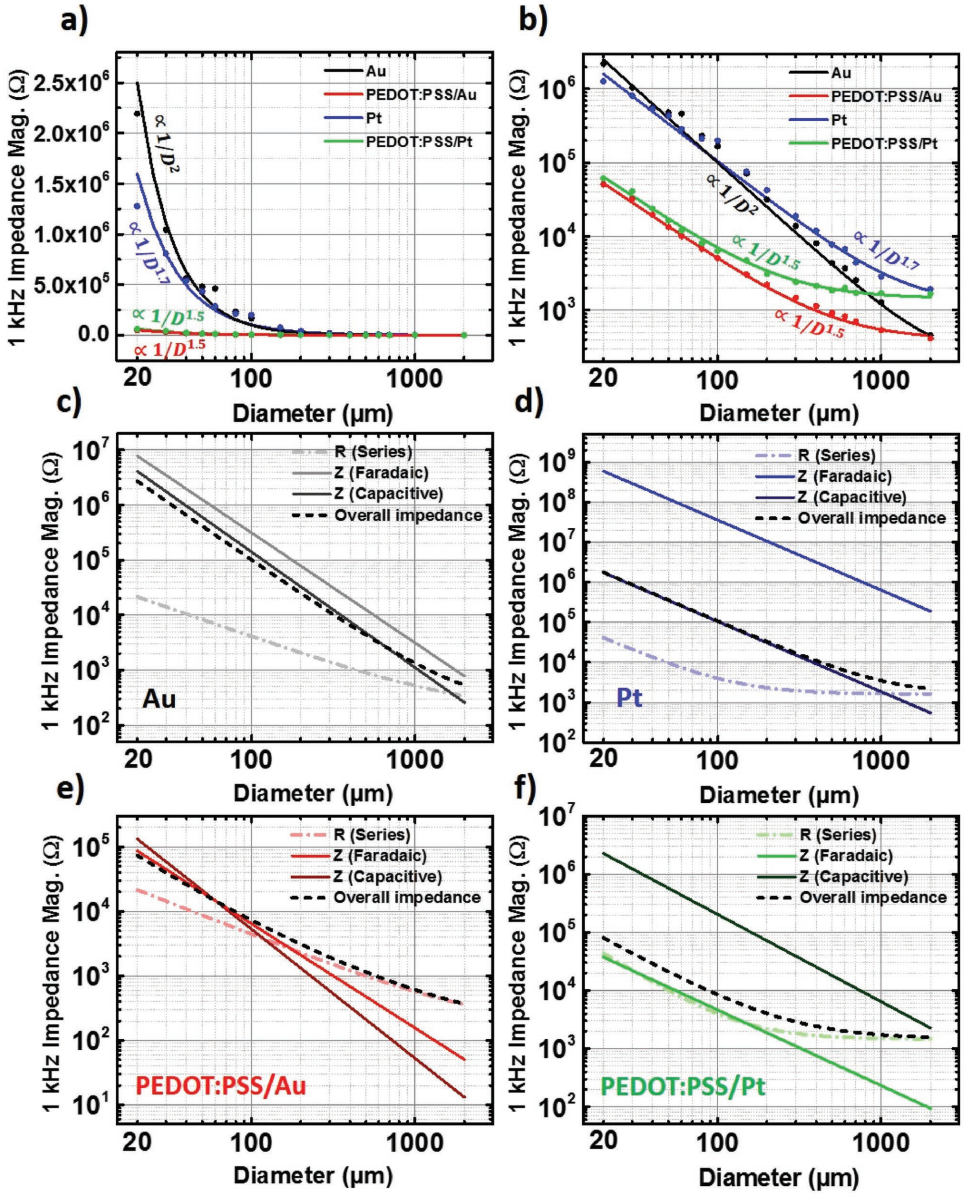


**Figure 5.** Contributions of each electrochemical element to the 1 kHz impedance as a function of contact size and material. Measured and fitted values of 1 kHz electrochemical impedances of scaled PEDOT:PSS/Au, PEDOT:PSS/Pt, Au, and Pt electrodes in a) semilog and b) log scale. Size dependence of each component of the electrochemical impedance plotted together with the overall 1 kHz impedance for c) Au, d) Pt, e) PEDOT:PSS/Au, and f) PEDOT:PSS/Pt.

dots converges to that of the underlying metal as the diameter increases to millimeter scales. For larger diameters, the electrochemical limiting factor is the series resistance, $R_s$, which we found to be dominated by the underlying metal contact in Figure 4a,b. The PEDOT:PSS coated electrodes exhibited a combined perimeter/area dependency of $1/D^{1.5}$, whereas the metal ones showed mostly area dependency of $1/D^2$ for Au and $1/D^{1.7}$ for Pt. The independent electrochemical coupling effects for faradaic, capacitive, and those of series resistance at 1 kHz are benchmarked against the overall impedance for each material in Figure 5c–f. For Au, at small diameters, the overall impedance is determined by the capacitive coupling ($Z_f$ is highest and overall $|Z|$ is equivalent to nearly $|X|_{CPE}$) until $|X|_{CPE}$ becomes lower than $R_s$ at larger diameters where the overall impedance becomes limited by $R_s$. For PEDOT:PSS on Au and Pt, and at 1 kHz, the series resistance becomes larger than the parallel combination of the capacitive and faradaic impedances at about 108 µm for PEDOT:PSS/Au and 106 µm for PEDOT:PSS/Pt and the overall impedance becomes dominated by $R_s$. The faradaic component for electrochemical coupling for Pt, embodied in a large $R_{ct}$, is ineffective at 1 kHz and capacitive coupling is efficient for all diameters.

For neural activity embodied in low frequency field potentials, it is important to analyze the size-dependent impedance at frequencies lower than 1 kHz. To do this, we extracted the impedance from the spectra of Figure 2 and plotted it at 1, 4, 8, 12, 40, 100, 500, and 1000 Hz in **Figure 6** as a function of diameter and in Figure S6 (Supporting Information) as a function of GSA. The intermediate frequency bands between these limits are known as the delta (Δ), theta ($\theta$), alpha ($\alpha$), beta ($\beta$), gamma ($\gamma$), high frequency oscillation, and single unit (SU). At lower frequencies, PEDOT:PSS on Au lead to over 18.4× lower impedances for all sizes compared to Au electrodes and about 4.8× lower impedances for PEDOT:PSS on Pt compared to Pt electrodes. Since the lower frequencies exhibit mainly a capacitive behavior for all diameters, a nearly $1/D^{1.75}$ dependence of the overall impedance was observed for PEDOT:PSS/Au and PEDOT:PSS/Pt (Figure S7, Supporting Information). At higher frequencies, and as the diameter increases and the $R_s$ starts to dominate, a slower dependence of $1/D^{1.5}$ for PEDOT:PSS/Au and $1/D^2$ for PEDOT:PSS/Pt was observed as noted in Figure 5. The phase spectra in Figure 5b–h demonstrate the relevant electrochemical coupling mechanism. For Au, the phase at all frequency bands is nearly capacitive and started to become a combination of capacitive/ohmic for diameters >1000 µm and at the higher frequencies. Lower frequency signals are coupled capacitively. For PEDOT:PSS/Au and PEDOT:PSS/Pt, smaller diameters exhibited capacitive coupling up to ≈100 µm, beyond which a mixed capacitive/ohmic coupling regime prevailed, becoming mostly ohmic at higher frequencies and larger diameters. This dependence is nearly reversed for Pt where the lower frequencies and smaller diameters exhibit mostly ohmic behavior and the larger diameter and larger frequencies exhibit a similar trend to Au, PEDOT:PSS/Au, and PEDOT:PSS/Pt where mixed capacitive/ohmic characteristics were observed.

The above discussion delineates the electrochemical interface properties that underlie the recording of brain waves using ECoG electrodes. An important consequence of electrode impedance associated with electrode size is the consequent noise level. Naturally, the lower impedance PEDOT:PSS electrodes exhibit low noise voltages that are limited to that of the amplifier (Tucker Davis Technologies, TDT) background noise voltage (**Figure 7**a). The macroscale Au and Pt electrodes also exhibit smaller noise voltages but as the diameter is reduced at or below 100 µm, the noise voltage rapidly increases above the amplifier background noise (Figure 7a). The root mean square (RMS) for the noise spectral density (NSD) in the 1 Hz to 10 kHz frequency band exhibited a $1/D^2$ dependence at smaller diameter for Pt and a $1/D^{1.7}$ dependence of Au, whereas for PEDOT:PSS/Au and PEDOT/Pt, the noise density scaled with $1/D^{0.9}$ and $1/D$, respectively, as illustrated in Figure 7c. The RMS noise spectral density scaling with geometrical surface area is shown in Figure S8 (Supporting Information). The noise power spectral density (PSD) for five different diameters (20, 60, 200, 500, and 1000 µm) as a function of frequency is plotted in Figure 7b. For all diameters, the noise spectra are limited to the amplifier noise with a slight $1/f$ noise component below 100 Hz. The Au noise power spectra also exhibited similar noise spectra to the amplifier for diameters larger than 500 µm. For diameters below 200 µm, the $1/f^{\alpha}$ noise power increases as the diameter decreases where $\alpha$, the Hooge coefficient,[11] was found to be equal to 1.6, 1.65, and 2 for diameter of 200, 60, and 20 µm, respectively. Also, the corner frequency, $f_c$, which denotes a change in the total noise dependence from $1/f$ noise to the frequency-independent thermal/white noise, increases for smaller diameters and was found to be 92 Hz for 200 µm, 102 Hz for 60 µm, and 115 Hz for 20 µm. For Pt, a similar trend was observed such that both $\alpha$ and $f_c$ increase as the diameter decreases. $\alpha$ was found to be equal to 1.65, 1.7, and 2.4, and $f_c$ equal to 103, 111, and 125 Hz for $D$ = 200, 60, and 20 µm, respectively. The ion transport in porous membranes was found to exhibit Hooge coefficients that are greater than or equal to ≈1.5.[12] We speculate that since the adsorption sites for ions on the Pt surface are nonhomogeneous and the charge coupling is capacitive that relies on ion diffusion, the Hooge factors for Pt are larger than those of Au electrodes for any given diameter. Overall, the low noise power density for PEDOT:PSS suggests that the SNR will not degrade as the diameter of ECoG devices is scaled to 20 µm suggesting that PEDOT:PSS has the highest potential for high spatiotemporal resolution among all ECoG microelectrode materials studied here.

In conclusion, we presented a systematic study of the scaling effects on the electrochemical properties of metallic Pt and Au and organic PEDOT:PSS electrodes. PEDOT:PSS electrodes exhibit better faradaic charge transfer and capacitive charge coupling than metal electrodes, and these characteristics lead to improved electrochemical performance and reduced noise at smaller electrode diameters. We found that PEDOT:PSS reduced the metal electrode impedances by up to 18× for electrodes with diameters <200 µm and the impedances became identical at millimeter scale due to dominance of series resistances particularly at higher frequencies. Therefore, the performance gains are especially significant at smaller diameters and lower frequencies where cognitive and clinical activities are usually observed in neuronal recordings. Additionally, the overall reduced noise of the PEDOT:PSS electrodes enables a lower noise floor for single unit activity recording. We believe

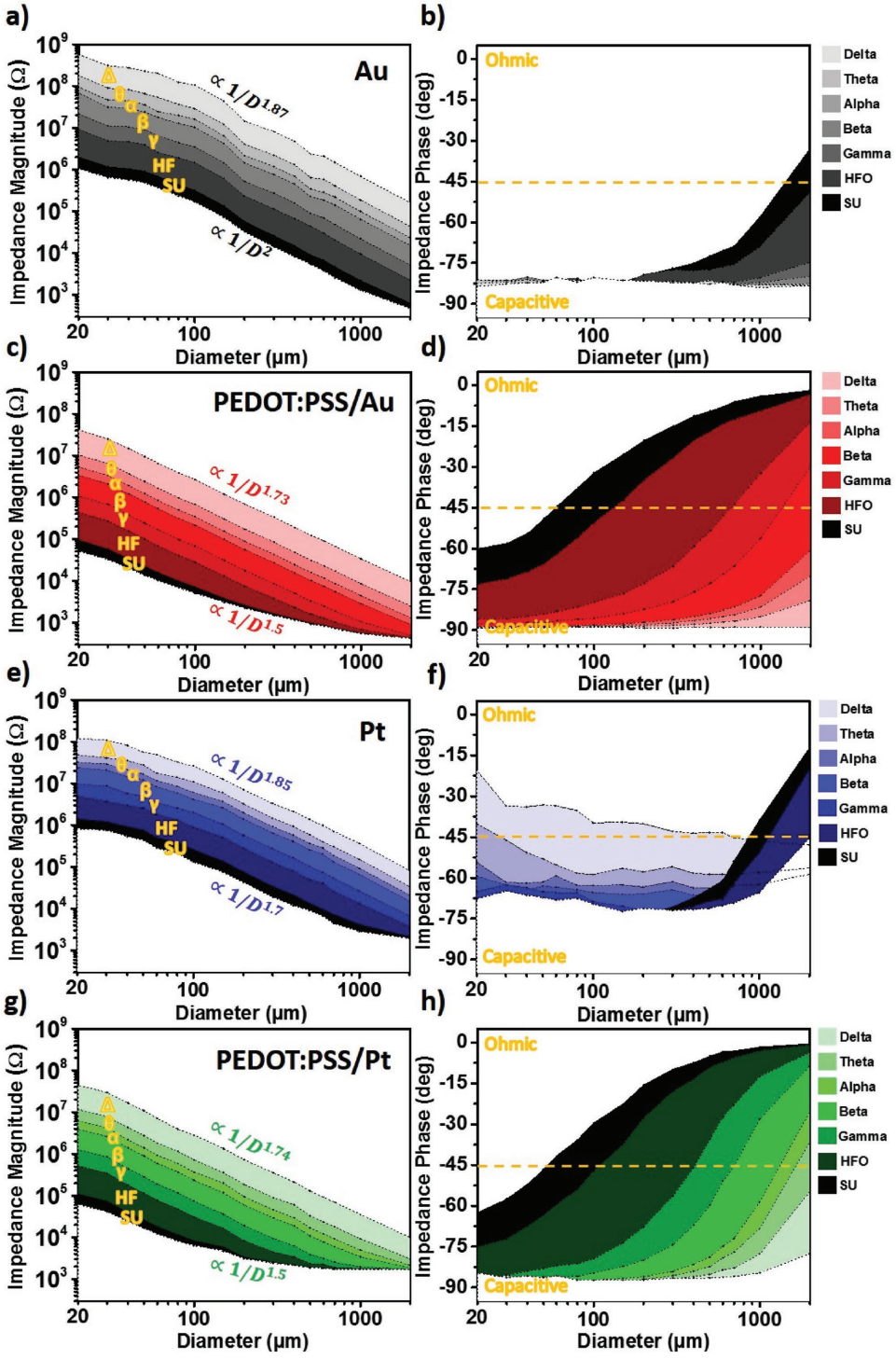


**Figure 6.** Electrochemical impedance spectra in different frequency bands relevant to ECoG brain signals plotted at 1–4 Hz, ($\Delta$, delta), 4–8 Hz ($\theta$, theta), 8–12 Hz ($\alpha$, alpha), 12–40 Hz ($\beta$, beta), 40–100 Hz ($\gamma$, gamma), 100–500 Hz (high frequency (HF)), and 500–1000 Hz (single units (SUs)). Impedance magnitude and phase diagrams as a function of diameter for a,b) Au electrodes, c,d) PEDOT:PSS/Au electrodes, e,f) Pt electrodes, and g,h) PEDOT:PSS/Pt electrodes.

that the detailed understanding of the electrochemical characteristics of these different materials and their scaling properties is of critical importance for the optimization of ECoG electrodes.

## 3. Experimental Section

*Device Fabrication*: The device fabrication is similar to previously established protocols[5,12] and is included here for completeness. Glass slides (Specialty Glass Products Inc.) were used as substrate carriers for

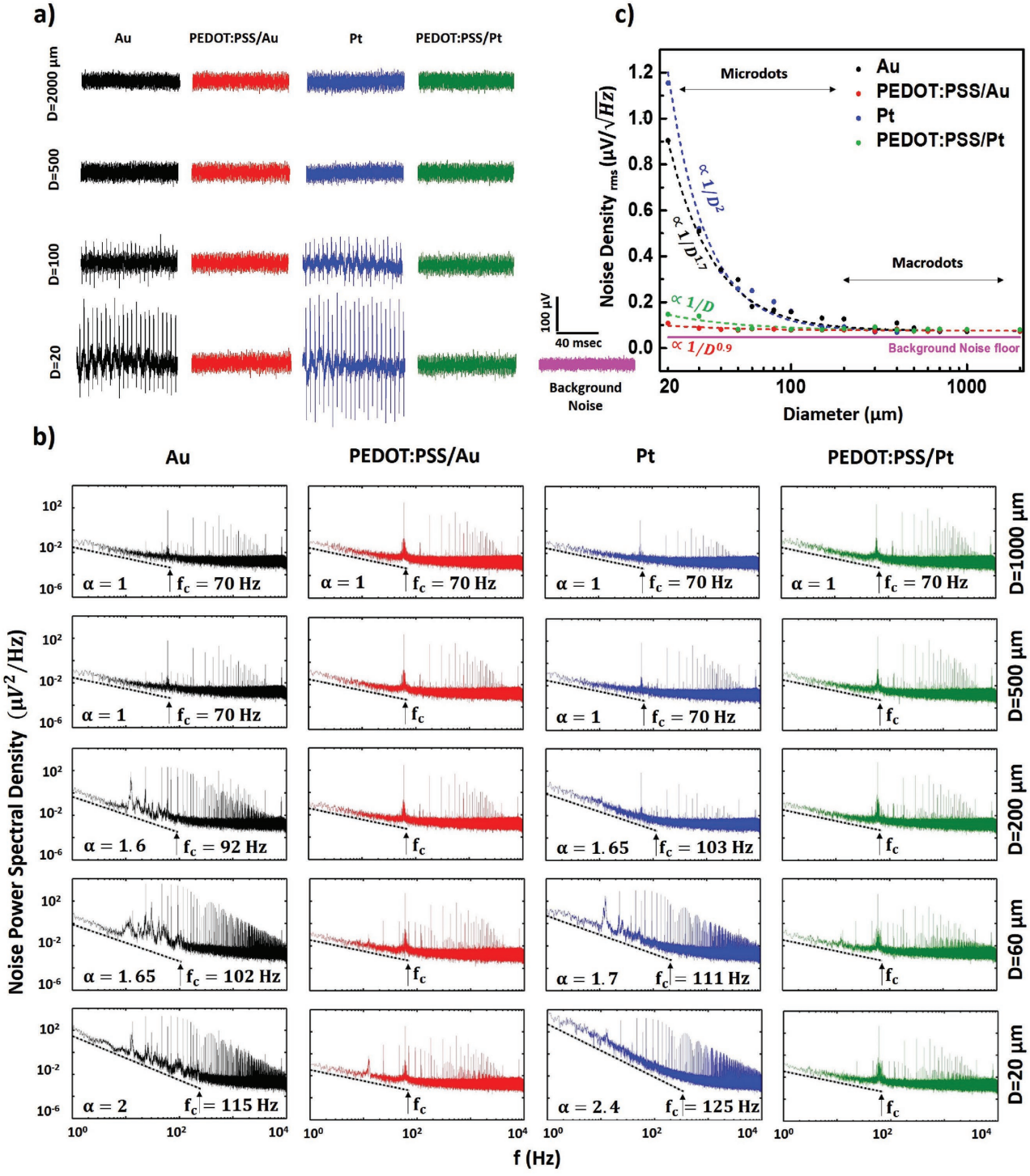


**Figure 7.** Effects of electrode diameter on noise performance for different electrode materials. a) Noise voltage–time traces (for a time duration of 100 ms) for Au (black), PEDOT:PSS/Au (red), Pt (blue), and PEDOT:PSS/Pt (green) with 20, 100, 500, and 2000 µm diameters. Purple color voltage–time trace is the amplifier noise. b) Noise power spectral densities for 20, 100, 500, and 1000 µm diameters. c) Calculated and fitted root-mean-square values of PSD in the 1 Hz–10 kHz frequency band as a function of diameter.

the thin parylene C layers. The glass slides were first solvent cleaned by rinsing with acetone/isopropanol (IPA)/deionized (DI) water/IPA, then were subjected to ultrasonic agitation in IPA for 5 min, and were then rinsed again with acetone/IPA/DI water/IPA. Diluted Micro-90 (0.1%), an anti-adhesion layer, was spun-cast at 1500 rpm on the glass slide to facilitate the separation of the device after the device fabrication was completed. A first parylene C layer (≈1.9 µm) was deposited by chemical vapor deposition using a PDS 2010 Parylene coater system. Metal lead patterns were defined and exposed using a Karl Suss MA6 mask aligner using NR9-3000 negative resist. Temescal BJD 1800 electron beam

evaporator was used for the deposition of 10 nm Ti adhesion layer and 100 nm Au contact layer, and the lift-off process in acetone followed. $O_2$ plasma (Oxford Plasmalab 80 RIE) was then applied for 2 min (150 W RF power) to activate the surface of parylene C for enhancing the adhesion of the subsequent encapsulating parylene C layer. An ≈ 1.9 µm parylene C layer was then deposited and followed by coating another Micro-90 anti-adhesion layer. This time, a slightly higher concentrated Micro-90 (1% as opposed to 0.1% for the first layer) was spun-cast at 650 rpm for 10 s on this second parylene C layer for ease of separation of the subsequent layers. A third parylene C layer was then deposited, followed by the spin-coating and patterning the thick 2010 SU-8 photoresist layer, which was exposed and developed with an SU-8 developer. $O_2$ plasma was used to etch the openings in the third and then second parylene C layers prior to the deposition of PEDOT:PSS. After the $O_2$ plasma etching step, the exposed Au surface was cleaned using moderate soniction while the device was immersed in DI water. 20 mL aqueous dispersion of PEDOT:PSS (PH 1000 from Clevios) was mixed with ethylene glycol (5 mL), dodecylbenzene sulfonic acid (50 µL), and 1 wt% of (3-Glycidyloxypropyl)trimethoxysilane, and the solution was spun-cast at 650 rpm for 30 s and prebaked at 95 °C for 1 min. The third parylene C layer was then mechanically peeled off in all regions except where PEDOT: PSS made contact with the Au surface on the microarray and macrodot regions. Finally, the devices were cured at 140 °C for 1 h and immersed in DI water to remove any Micro-90 residue from the PEDOT:PSS and parylene C surface. Fabrication of the metral (Pt and Au) microarrays followed a similar procedure to that of PEDOT:PSS devices except for the PEDOT:PSS deposition, which was not carried out. For the Pt devices, a 10 nm Ti adhesion layer and 100 nm Pt contact layer were deposited by sputtering.

*Device Characterization*: The devices were imaged using an FEI SFEG ultra high resolution SEM at 10 kV accelerating voltage. To reduce electron charging in the specimen, a 15 nm thick Ti layer was deposited on the back of the device and was electrically connected to the stage of the system providing a runaway path for impnging electrons. EIS was performed using a GAMRY interface 1000E in phosphate buffer saline (PBS) solution, using three electrodes configuration, i.e., Ag/AgCl electrode as a reference electrode, a large platinum electrode as a counter electrode, and target microarray/macrodot arrayes as the working electrode. Sinusoidal signals with 10 mV RMS AC voltage and zero DC bias were applied and the frequency was swept from 1 Hz to 10 kHz. Noise measurement was perfomed using TDT acqusition system (RZ2 BioAmp Processor), whereas the electrode arrays were immersed in PBS solution, and 120 s duration multiplexed measurements were carried out on different channels with 24 kHz sampling rate per channel. RMS noise values were obtained by taking the standard deviation of each channel's voltage–time trace after filtering from 1 Hz to 10 kHz with a third order Butterworth filter (no additional notch filter was applied). The NSD was obtained from the raw data using the Welch periodogram estimation method. After filtering from 1 Hz to 10 kHz, RMS noise values were obtained from each electrode's PSD.

*Electrochemical Impedance Fitting*: A custom-made fitting algorithm was developed to fit using Matlab both the Nyquist and Bode plots of each measured EIS to equivalent impedance of the circuit configurations shown in Figure 3a. The input to the fitting algorithm is initial guess for the expected range of respective electrochemical component of the equivalent circuits in Figure 3a. The code runs to minimize the error between the model's impedance and the experimental impedance of the electrodes resulting in best-match parameter values at the minimum error for the proposed circuit model. The fits for the extracted EIS electrochemical components were carried out using built-in Power functions in Origin software package.

## Supporting Information

Supporting Information is available from the Wiley Online Library or from the author.

## Acknowledgements

S.A.D. led the project and coordinated the efforts, designed the experiments, interpreted the results, wrote the manuscript, and received feedback from all co-authors. M.G. fabricated the devices, carried out the electrochemical characterization, fitted the data, interpreted the results, and co-wrote the manuscript. A.T.E. carried out the fits in Figure 3. A.T. did the FIB slicing and SEM imaging. This work was graciously supported by the Center for Brain Activity Mapping (CBAM) at UC San Diego. S.A.D. and V.G. acknowledge faculty start-up support from the Department of Electrical and Computer Engineering at UC San Diego. S.A.D. acknowledges partial support from the NSF (Grant No. ECCS-1351980). V.G. acknowledges partial support from the University of California Multicampus Research Programs and Initiatives (UC MRPI) (Grant No. MR-15-328909). E.H. acknowledges partial support from the Office of Naval Research (Grant No. N00014-13-1-0672).

## Conflict of Interest

The authors declare no conflict of interest.

## Keywords

diameters, electrocorticography, PEDOT:PSS, scaling, sizes

Received: June 4, 2017
Revised: July 27, 2017
Published online:

[1] a) D. R. Kipke, W. Shain, G. Buzsáki, E. Fetz, J. M. Henderson, J. F. Hetke, G. Schalk, *J. Neurosci.* **2008**, *28*, 11830; b) G. Buzsáki, *Nat. Neurosci.* **2004**, *7*, 446.

[2] a) S. F. Cogan, *Annu. Rev. Biomed. Eng.* **2008**, *10*, 275; b) W. Franks, I. Schenker, P. Schmutz, A. Hierlemann, *IEEE Trans. Biomed. Eng.* **2005**, *52*, 1295.

[3] N. G. Hatsopoulos, J. P. Donoghue, *Annu. Rev. Neurosci.* **2009**, *32*, 249.

[4] a) K. Najafi, J. Ji, K. Wise, *IEEE Trans. Biomed. Eng.* **1990**, *37*, 1; b) K. A. Ludwig, N. B. Langhals, M. D. Joseph, S. M. Richardson-Burns, J. L. Hendricks, D. R. Kipke, *J. Neural Eng.* **2011**, *8*, 014001.

[5] a) M. Sessolo, D. Khodagholy, J. Rivnay, F. Maddalena, M. Gleyzes, E. Steidl, B. Buisson, G. G. Malliaras, *Adv. Mater.* **2013**, *25*, 2135; b) D. Khodagholy, T. Doublet, M. Gurfinkel, P. Quilichini, E. Ismailova, P. Leleux, T. Herve, S. Sanaur, C. Bernard, G. G. Malliaras, *Adv. Mater.* **2011**, *23*, H268; c) D. Khodagholy, J. N. Gelinas, T. Thesen, W. Doyle, O. Devinsky, G. G. Malliaras, G. Buzsáki, *Nat. Neurosci.* **2015**, *18*, 310; d) D. Khodagholy, J. N. Gelinas, Z. Zhao, M. Yeh, M. Long, J. D. Greenlee, W. Doyle, O. Devinsky, G. Buzsáki, *Sci. Adv.* **2016**, *2*, e1601027; e) J. Hermiz, N. Rogers, E. Kaestner, M. Ganji, D. Cleary, J. Snider, D. Barba, S. Dayeh, E. Halgren, V. Gilja, *Proceedings of the 2016 IEEE 38th Annual Int. Conf.*, Orlando, FL, **2016**, 4511–4514. f) I. Uguz, M. Ganji, A. Hama, A. Tanaka, S. Inal, A. Youssef, R. M. Owens, P. P. Quilichini, A. Ghestem, C. Bernard, *Adv. Healthcare Mater.* **2016**, *5*, 3094.

[6] J. Rivnay, S. Inal, B. A. Collins, M. Sessolo, E. Stavrinidou, X. Strakosas, C. Tassone, D. M. Delongchamp, G. G. Malliaras, *Nat. Commun.* **2016**, *7*, 11287.

[7] J.-W. Jeong, G. Shin, S. I. Park, K. J. Yu, L. Xu, J. A. Rogers, *Neuron* **2015**, *86*, 175.

 

[8] G. Buzsáki, C. A. Anastassiou, C. Koch, *Nat. Rev. Neurosci.* **2012**, *13*, 407.
[9] X.-Z. R. Yuan, C. Song, H. Wang, J. Zhang, *Electrochemical Impedance Spectroscopy in PEM Fuel Cells: Fundamentals and Applications*, Springer Science & Business Media, London, UK, **2009**.
[10] M. Ganji, E. Kaestner, J. Hermiz, N. Rogers, A. Tanaka, D. Cleary, S. H. Lee, J. Snider, M. Halgren, G. R. Cosgrove, B. S. Carter, D. Barba, I. Uguz, G. G. Malliaras, S. S. Cash, V. Gilja, E. Halgren, S. A. Dayeh, *Adv. Funct. Mater.* **2017**, *27*, 1700323.
[11] F. Hooge, *Phys. Lett. A* **1970**, *33*, 169.
[12] E. Frehland, *Biophys. Chem.* **1978**, *8*, 255.

ADVANCED FUNCTIONAL MATERIALS

# Supporting Information

for *Adv. Funct. Mater.*, DOI: 10.1002/adfm.201703018

# Scaling Effects on the Electrochemical Performance of poly(3,4-ethylenedioxythiophene (PEDOT), Au, and Pt for Electrocorticography Recording

*Mehran Ganji, Ahmed T. Elthakeb, Atsunori Tanaka, Vikash Gilja, Eric Halgren, and Shadi A. Dayeh**

Supporting Information

# Scaling Effects on the Electrochemical Performance of PEDOT, Au, and Pt for Electrocorticograpy Recording

*Mehran Ganji,* Ahmed T. Elthakeb, *Atsunori Tanaka, Vikash Gilja, Eric Halgren and Shadi A. Dayeh**

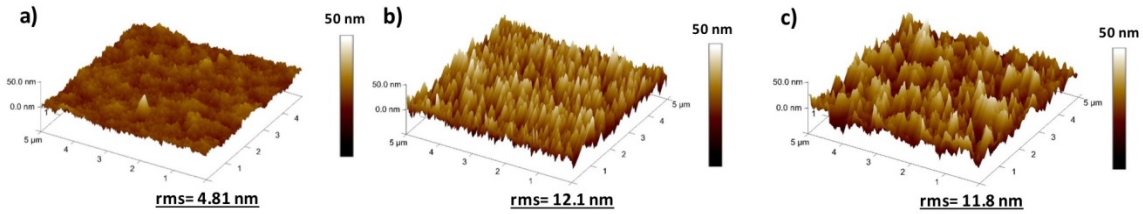


**Figure S1:** Atomic Force Microscopy images and roughness root-mean-square values of 5×5 $\mu m^2$ scanned area of (a) PEDOT:PSS/Au, (b) Pt, and (c) Au electrode surfaces.

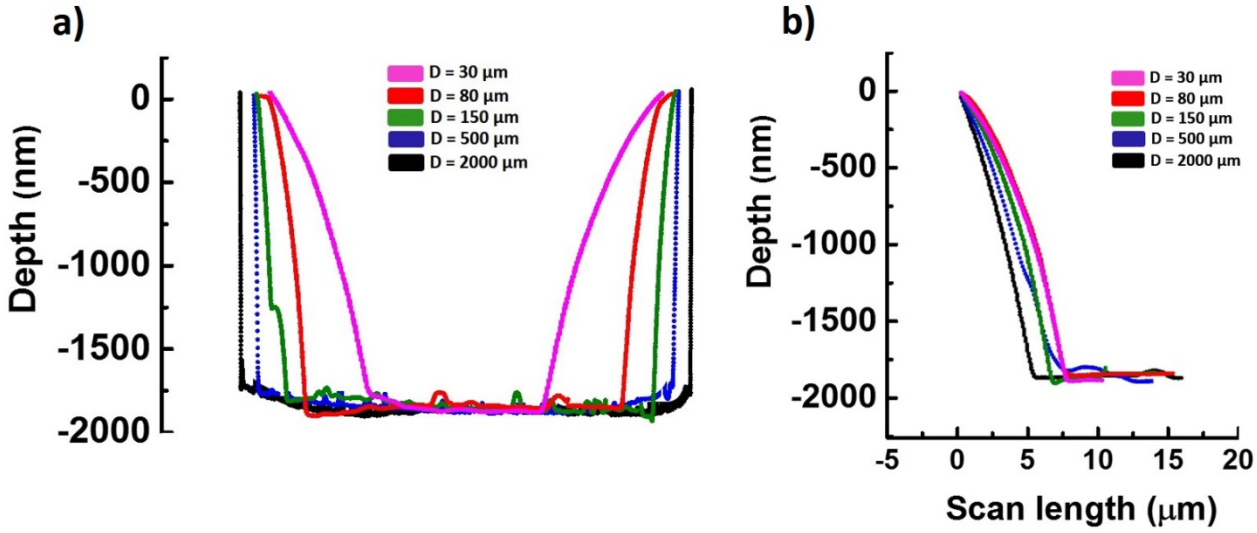


**Figure S2. Depth and edge profile of PEDOT:PSS/Au electrodes. (a)** Dektak scan profiles of 30, 80, 150, 500 and 2000 µm diameter electrodes showing the depth of the PEDOT at the center of the electrode is ~ 1.9 µm below the parylene C surface for all electrodes. The x-axis is not plotted to scale to enable viewing of the depth for all electrodes. **(b)** Edge profile of 30, 80, 150, 500 and 2000 µm diameter electrodes plotted to scale as a function of distance from the electrode edge. The difference in the edge profile is nearly identical for all dots.

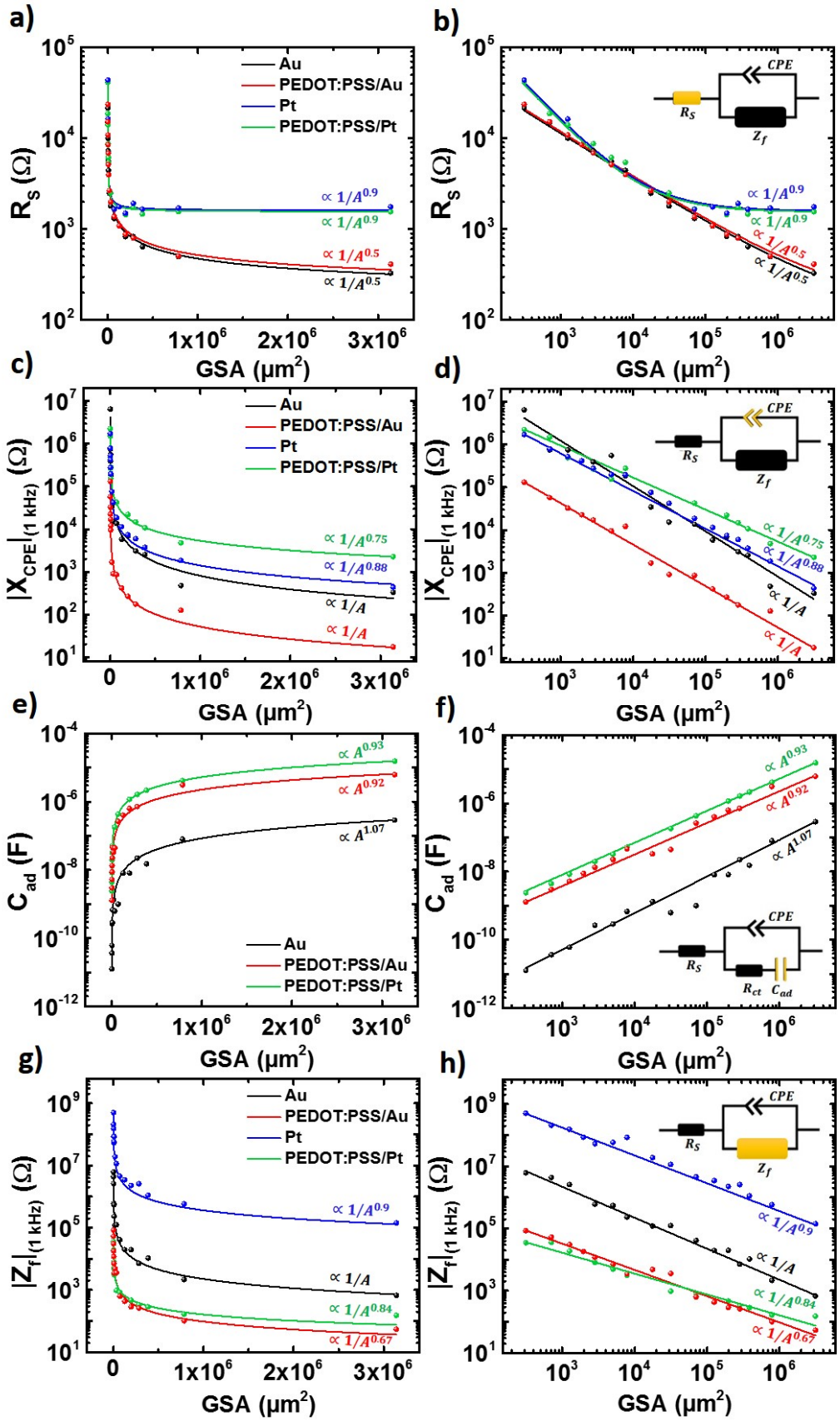
a)
b)
c)
d)
e)
f)
g)
h)
Au
PEDOT:PSS/Au
Pt
PEDOT:PSS/Pt
$R_S$ (Ω)
$|X_{CPE}|_{(1\ kHz)}$ (Ω)
$C_{ad}$ (F)
$|Z_f|_{(1\ kHz)}$ (Ω)
GSA (μm²)
CPE
$R_S$
$Z_f$
$R_{ct}$
$C_{ad}$
$\propto 1/A^{0.9}$
$\propto 1/A^{0.5}$
$\propto 1/A^{0.75}$
$\propto 1/A^{0.88}$
$\propto 1/A$
$\propto A^{0.93}$
$\propto A^{0.92}$
$\propto A^{1.07}$
$\propto 1/A^{0.84}$
$\propto 1/A^{0.67}$

**Figure S3: Effects of electrode geometrical surface area on specific electrochemical components of the electrode interface**. **(a, b)** Series resistance is greater for large GSA Pt electrodes (blue and green lines compared to red and black), independent of PEDOT:PSS coating (red vs. black, green vs. blue lines). **(c, d)** CPE reactance at 1 kHz is least for PEDOT:PSS/Au electrodes at all GSA. **(e, f)** Adsorption capacitance is increased in PEDOT:PSS coated contacts. **(g, h)** Faradaic branch impedance (at 1 kHz) capacitance is decreased in PEDOT:PSS coated contacts. Extracted and fitted values are shown in semilog **(a, c, e, g)** and log **(b, d, f, h)** scales.

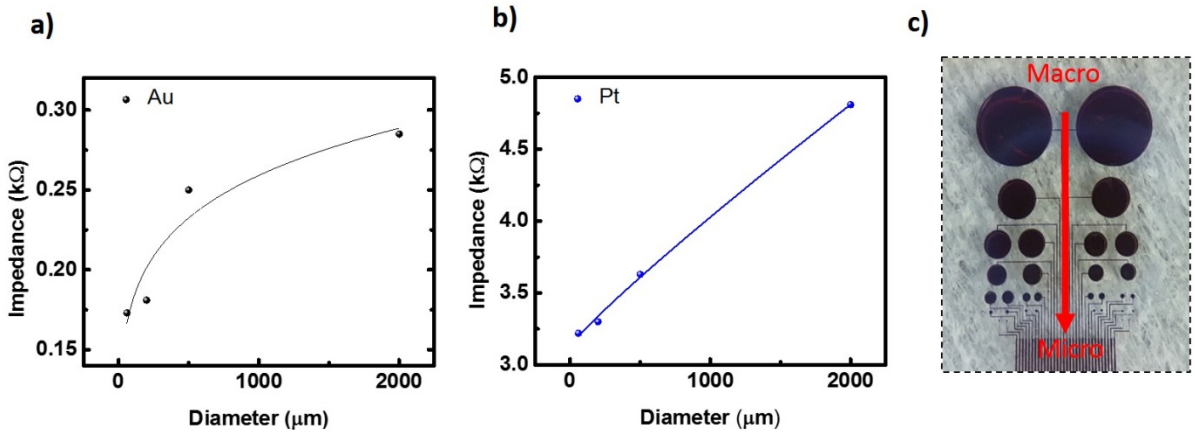


**Figure S4. Metal lead resistance measurements by 2-point probe.** Metal lead series resistance of 60, 200, 500 and 2000 μm diameter electrodes for Au **(a)** and Pt **(b)** measured by placing probes on electrode surface and pads. **(c)** Optical image of devices layout showing the macrodots have longer leads compared to microdots and this excess length leads to a slightly higher series resistance. Of note is that the measured resistances for the devices characterized in the main text are lower than these two devices characterized here for the series resistance effects.

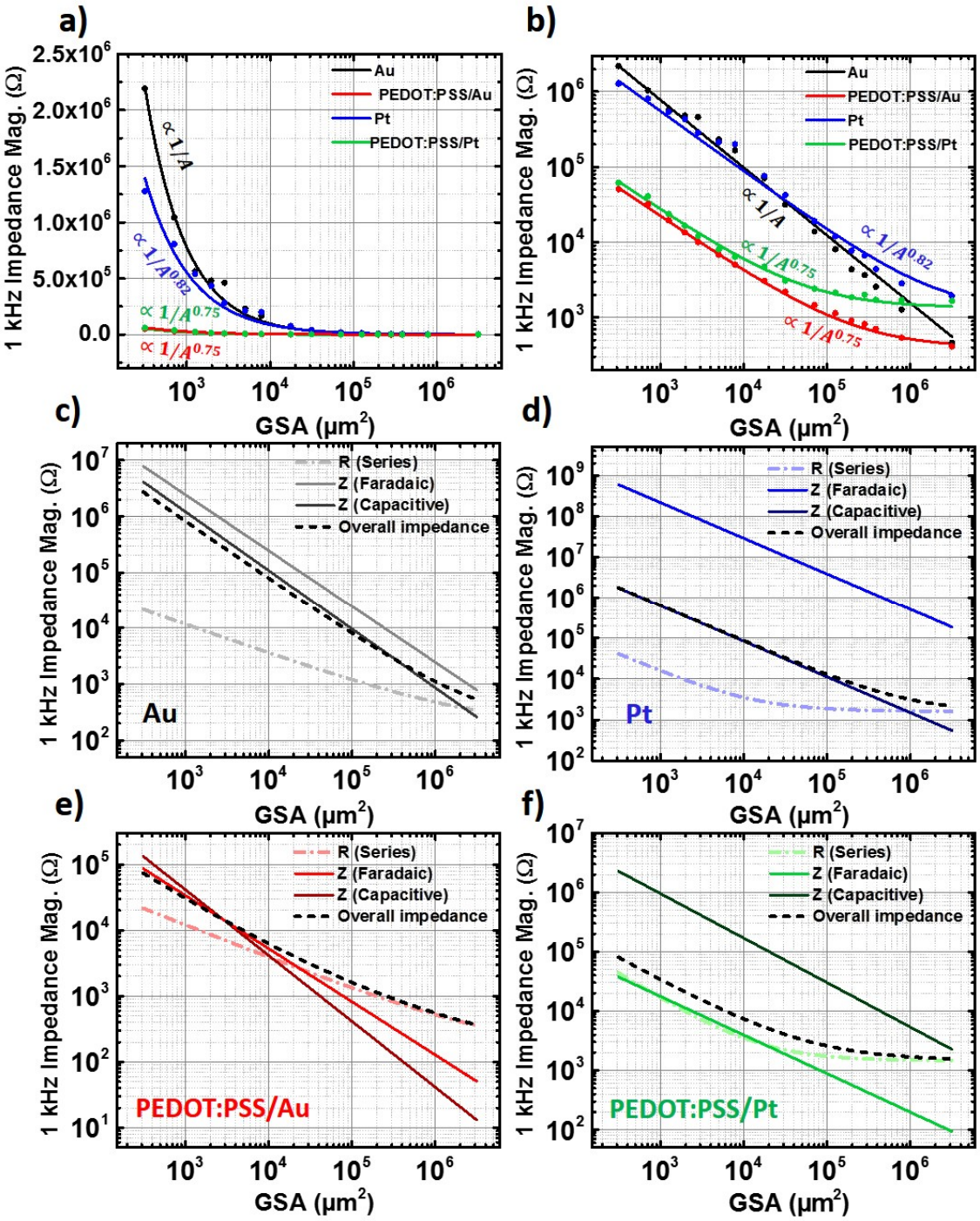


**Figure S5. Contributions of each electrochemical element to the 1 kHz impedance as a function of GSA and material.** Measured and fitted values of 1 kHz electrochemical impedances of scaled PEDOT:PSS/Au, PEDOT:PSS/Pt, Au and Pt electrodes in semilog **(a)** and log **(b) scale .**GSA dependence of each component of the electrochemical impedance plotted together with the overall 1 kHz impedance for Au **(c)**, Pt **(d)**, PEDOT:PSS/Au **(e)** and PEDOT:PSS/Pt **(f)**.

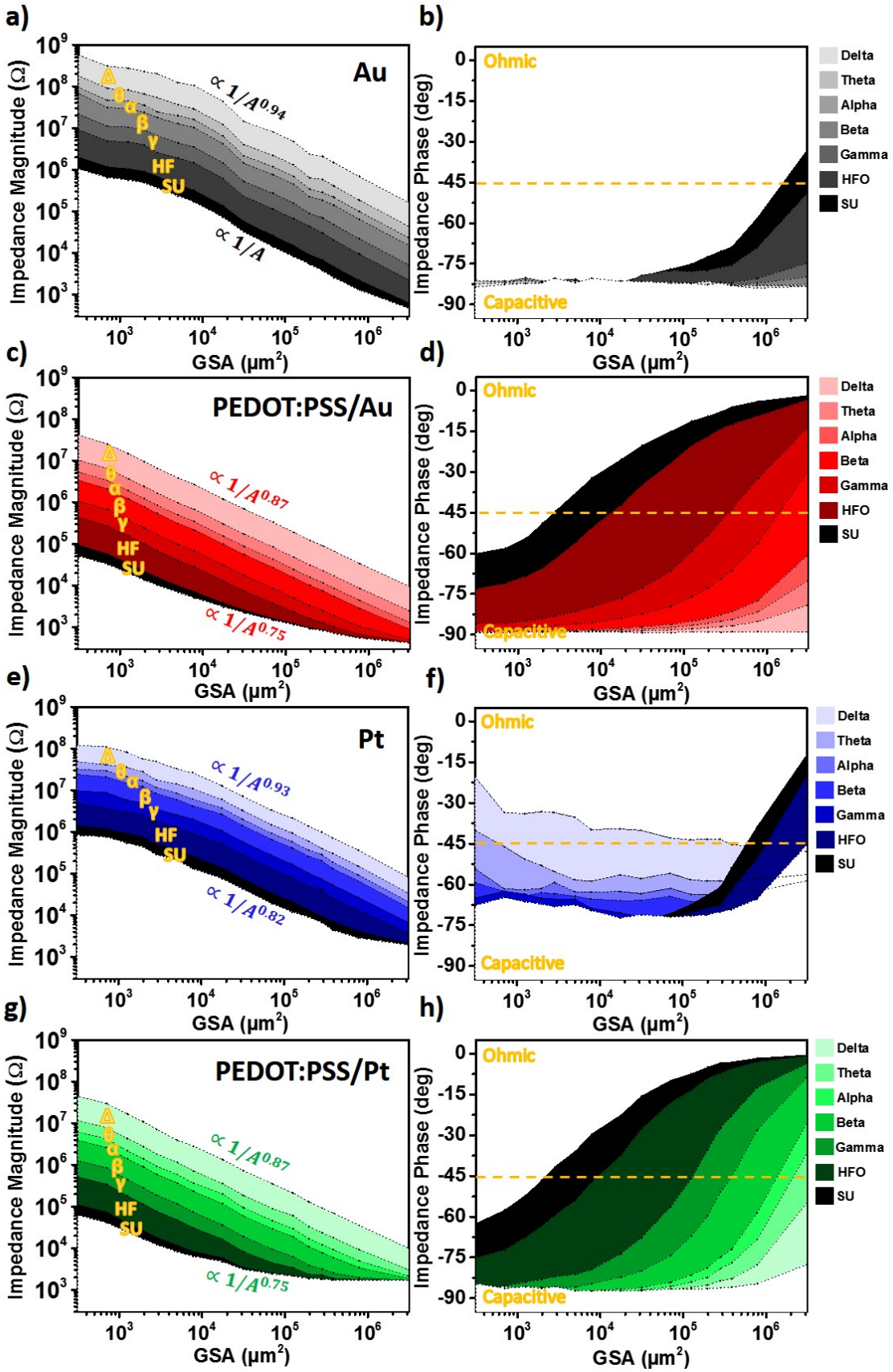
a)
b)
c)
d)
e)
f)
g)
h)
Au
PEDOT:PSS/Au
Pt
PEDOT:PSS/Pt
Impedance Magnitude (Ω)
Impedance Phase (deg)
GSA (μm²)
Δ
θ
α
β
γ
HF
SU
∝ 1/A^0.94
∝ 1/A
∝ 1/A^0.87
∝ 1/A^0.75
∝ 1/A^0.93
∝ 1/A^0.82
Ohmic
Capacitive
Delta
Theta
Alpha
Beta
Gamma
HFO
SU

**Figure S6. Electrochemical impedance spectra in different frequency bands relevant to ECoG brain signals plotted at 1-4 Hz, (Δ, delta), 4-8 Hz (θ, theta), 8-12 Hz (α, alpha), 12-40 Hz (β, betta), 40-100 Hz (γ, gamma), 100-500 Hz (HF, high frequency) and 500-1000 Hz (SU, single units).** Impedance magnitude and phase diagrams as a function of GSA for Au electrodes **(a)** and **(b)**, PEDOT:PSS/Au electrodes **(c)** and **(d)**, Pt electrodes **(e)** and **(f)** and PEDOT:PSS/Pt electrodes **(g)** and **(h)**.

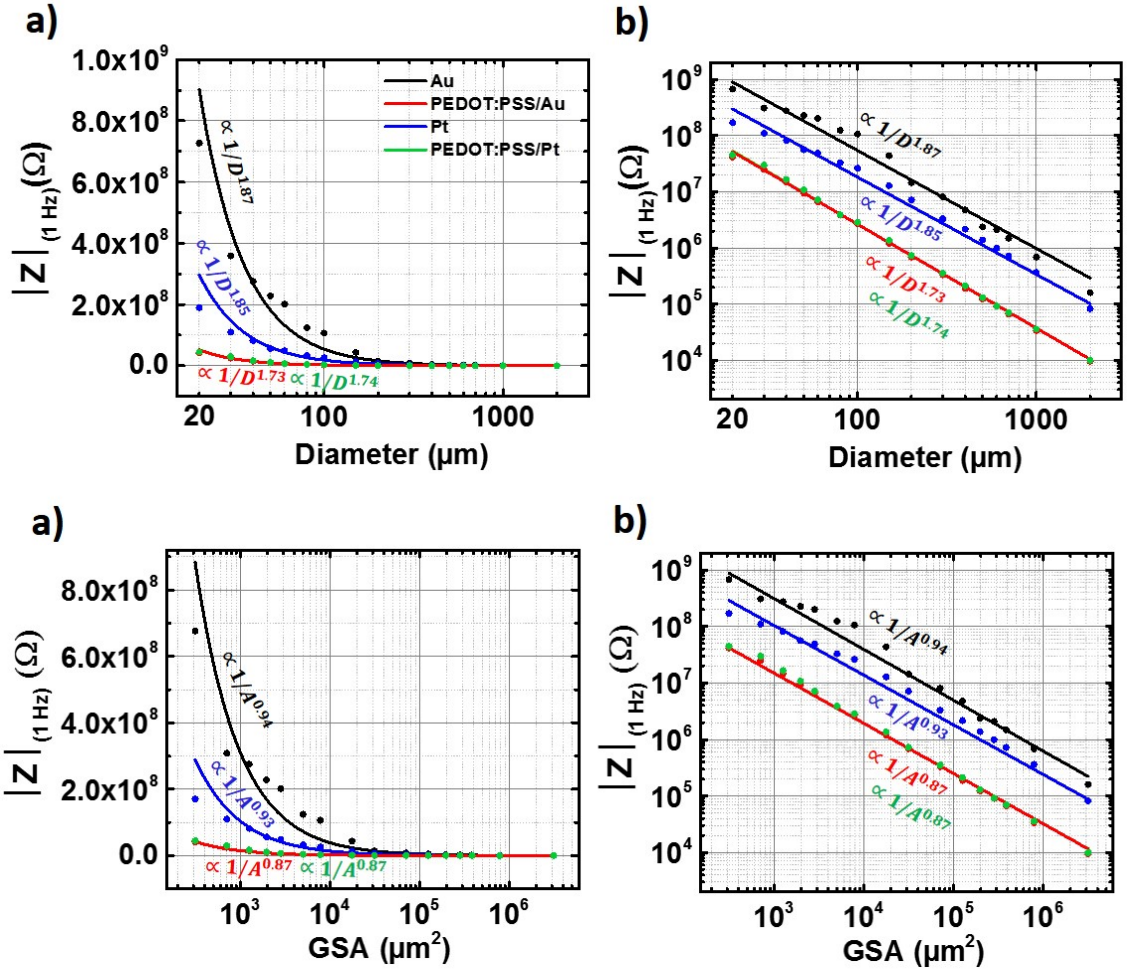


**Figure S7. Fits for the diameter-dependent impedances at 1 Hz.** Measured and fitted values of 1 Hz electrochemical impedances of PEDOT:PSS/Au, PEDOT:PSS/Pt, Au and Pt electrodes plotted in linear **(a)** and log **(b)** scales. Top is plotted as a function of diameter. Bottom is plotted as a dunction of GSA.

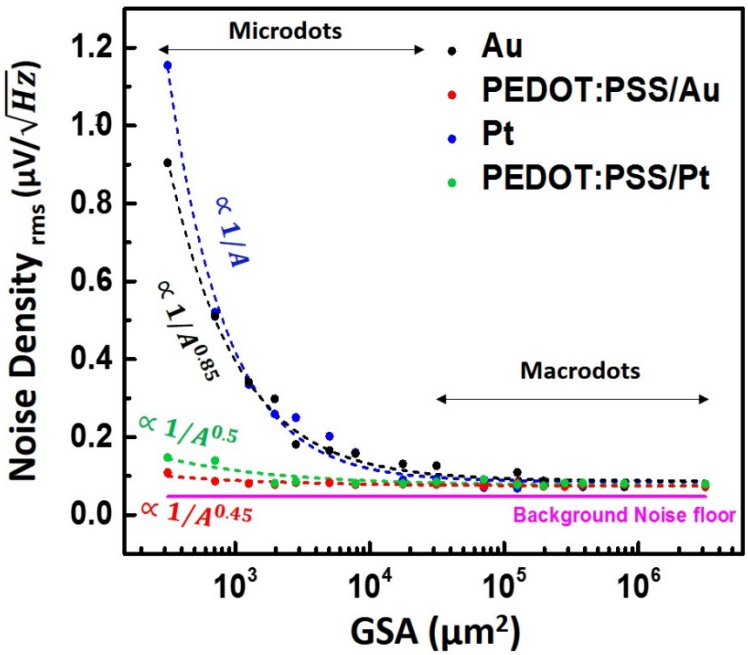


**Figure S8.** Calculated and fitted root-mean-square values of PSD in the 1 Hz- 10 kHz frequency band as a function of geometrical surface area (GSA).